Research Square

Preprints are preliminary reports that have not undergone peer review.
They should not be considered conclusive, used to inform clinical practice,
or referenced by the media as validated information.

Low oxygen-enriched reverse gasification of lignite: syngas composition, calorific value and multi-phase pollutant behaviour

Yulong Li
Guizhou bureau of geology and mineral development
Zhengyun Jiang
Guangzhou College of Technology and Business, Fanhu Economic Development Zone
Lei Qian
Guangzhou College of Technology and Business, Fanhu Economic Development Zone
Lingxia Wang
llzmnb@163.com

Guizhou bureau of geology and mineral development

Article

Keywords: Underground coal gasification, Lignite, Oxygen enrichment, Syngas quality, H_2S, Pollutant streams

Posted Date: November 26th, 2026

DOI: https://doi.org/10.21203/rs.3.rs-11764383/v1

License: This work is licensed under a Creative Commons Attribution 4.0 International License. Read Full License

Additional Declarations: No competing interests reported.

Abstract

Oxygen-enriched underground coal gasification (UCG) in the low-enrichment range (21–35% O_2) offers a practical route to improve syngas calorific value without the cost and handling burden of high-purity oxygen, yet coupled gas-quality and pollutant-release behaviour in this window remains sparsely characterised. This study reports a 69-h, ten-stage reverse-combustion experiment in a 5-m three-dimensional lignite simulator, covering air-blown baseline operation and 35% oxygen enrichment at 10, 15, 20 and 25 Nm³/h. Syngas composition and net calorific value were derived from metered flow and daily-calibrated gas chromatography; condensed-water chemistry (pH, COD, NH_3-N, oil, volatile phenols, ions) and crude-gas H_2S/tar were monitored at every stage, with sampling volume, condensate mass and gas throughput reported so that concentrations are not interpreted as total emission fluxes. Under 35% O_2, syngas net calorific value increases from 2.27–2.76 to 5.98 MJ/Nm³, while specific oxygen consumption falls to 42.8 Nm³/GJ at the 10 Nm³/h enriched setting. H_2S concentration peaks at 1464 mg/m³ in the 15 Nm³/h enriched case, and condensed-water organic loads rise with flow rate and enrichment. A min–max normalised screen over gasification efficiency, oxygen-supply cost and environmental risk identifies a weight-dependent compromise rather than a statistically established optimum. The work provides a transparent experimental dataset for assessing low-oxygen-enriched UCG as a syngas-producing and pollutant-generating process, and underscores that improved gas quality does not imply reduced total pollutant release.

Highlights

• 69-h reverse UCG test maps the 21–35% oxygen-enrichment window.

• Syngas NCV rises to 5.98 MJ/Nm³ at 35% O_2 and 20 Nm³/h.

• H_2S peaks at 1464 mg/m³; concentrations, not fluxes, are reported.

• Tripartite screening gives a weighted compromise, not a statistical optimum.

1. Introduction

Oxygen-enriched underground coal gasification (UCG) presents a narrow yet practically significant trade-off between process efficiency and environmental impact (Su et al. 2025 and Ding et al., 2024). Elevating the oxygen partial pressure enhances the calorific value of the product gas and diminishes the specific oxygen consumption per unit energy output (Dong et al., 2026a). In contrast, elevated oxygen levels induce higher peak reaction temperatures, which accelerate both tar cracking and sulfur evolution, while concurrently augmenting the economic burden of enriched oxidant supply (Dong et al., 2026b and Huang et al., 2021). Despite the industrial relevance of UCG, existing literature is predominantly confined to two extreme scenarios: air-blown longwall gasification and high-purity oxygen gasification (≥ 40% O_2) (Perkins & Vairakannu, 2017). Field trials at Huating Coal Mine tested discrete oxygen-enrichment levels (21%, 32%, 42% and 100% O_2) and identified 30–40% O_2 as the optimal band for syngas calorific value (Wang et al., 2011), yet reported only isolated operating points without continuous gradient mapping or coupled multi-phase pollutant monitoring. The present 69-h, 5-m simulator campaign resolves exactly this low-oxygen-enrichment window (35% O_2, 15–20 Nm³/h). Furthermore, concurrent monitoring of product-gas quality and multi-phase pollutant release within a single integrated test

campaign is scarce. Consequently, improvements in gas quality are frequently evaluated in isolation, without systematic accounting for environmental emissions (Pankiewicz-Sperka et al., 2021).

This study is motivated by three specific research gaps. First, current low-oxygen trials typically report either net calorific value (NCV) or individual gas species, yet few studies synchronously derive both NCV and specific oxygen consumption from identical, metered flow data, limiting a self-consistent assessment of oxygen economy. Second, pollutants in wastewater and crude syngas are often documented in separate investigations, frequently omitting essential metadata such as sampling volume and condensate mass. This absence precludes differentiation between variations in pollutant concentration and total pollutant emission, thereby obscuring the true environmental footprint. Third, multi-criteria assessments in the literature rarely specify normalisation procedures or weighting schemes. Consequently, the reported optimal operating conditions lack reproducibility and cannot be re-evaluated under alternative priority frameworks, such as those imposing stringent environmental constraints.

To address these gaps, this work focuses on three key aspects through a 69-h reverse-combustion test conducted in a 5-m lignite simulator, comprising ten sequential stages across the 21–35% oxygen range: (1) the evolution of syngas quality and oxygen economy across this oxygen window; (2) the variation of pollutant concentrations in condensate water and crude syngas within the same interval; and (3) the performance ranking derived from a three-criterion screening framework with transparent and reproducible weighting. This constitutes an exploratory investigation of feasible operating windows. No replicate tests were performed; all stages proceeded sequentially within the same reactor. Consequently, no significance tests or uncertainty intervals are provided. Although condensate mass and gas flowrate were documented, recovery correction was not applied to all measured species. Therefore, this study does not conclude that oxygen enrichment reduces total pollutant release; only concentration-based trends observed during this campaign are discussed. Full operational constraints and uncertainty qualifications are provided in the Methods section.

2. Experimental system, test programme and sampling

2.1 Large-scale physical-simulation apparatus and similarity design

Most existing experimental simulations of reverse gasification rely on compact one-dimensional channels, which are inadequate for capturing the multi-physics coupling behaviour characteristic of field conditions. To overcome this limitation, the present study employed a 5-m-scale three-dimensional simulation furnace. The design was governed by established dimensionless similarity criteria, specifically homochronity (Ho), Froude (Fr), Euler (Eu), and Reynolds (Re) (Bazaluk et al., 2021).

The furnace base was covered with a 50-mm loess layer to act as a water-impermeable barrier. A cuboid lignite seam (4000 mm × 600 mm × 600 mm) was built inside the furnace, with a 50 mm × 50 mm square gasification channel pre-formed at the centre of the seam base. To maintain structural integrity, gaps between adjacent coal lumps were packed tight and sealed with a coal-powder slurry, as shown in Fig. 1.

During assembly, inlet and outlet pipelines were pre-installed. A total of 96 thermocouples were arranged in three vertical layers (upper, middle, and lower positions) within the coal seam to monitor temperature evolution; the

layout is presented in Fig. 2. An electric ignition wire was positioned horizontally inside the gasification channel, 300 mm from the inlet flow channel, and surrounded by combustible wood to facilitate seam ignition. A roof layer of refractory cement was then constructed above the coal seam, incorporating eight additional thermocouples evenly distributed across its surface. Loess was subsequently filled and compacted above the roof layer to complete the assembly.

The apparatus preserves the sequential progression of a reverse-combustion process (injection, oxidation zone, gasification channel) at a length scale amenable to detailed instrumentation. However, it is not intended as a geometrically scaled model of a field seam; the limitations of similarity are discussed in Section 4.2.

2.2 Coal-quality characteristics of the test lignite

Coal samples were collected from an active UCG field test site with approval from both mine management and the project team. All sampling procedures complied with on-site safety regulations and relevant mining management requirements; no commercial transfer of samples occurred.

Table 1
Proximate and ultimate analyses of the coal sample.

Industrial analysis/%				**Elemental analysis /%**				
M_{ad}	A_{ad}	V_{ad}	FC_{ad}	C_{daf}	H_{daf}	O_{daf}	N_{daf}	S_{daf}
10.09	13.97	38.3	47.64	69.61	3.879	13.9	0.87	0.38

2.3 Full-time-sequence operating-condition design

The total test duration was 69 h, during which ten consecutive time-sequential operating cases were implemented, covering ignition, graded air supply, graded 35% oxygen enrichment and final purging. Three levels of gasification-agent flow rates (low, medium and high) were adopted so that the performance of the air-blown and low-oxygen-enrichment processes could be compared comprehensively. A layered sampling strategy was employed upon completion of the test: roof-soil samples were collected every 30 cm and residual-coal samples every 50 cm along the strike direction of the coal seam. In parallel, the profile dimensions of the gasification cavity were measured, and physical characteristics such as roof subsidence, local coking and pipeline corrosion were documented. This strategy addresses the deficiency of existing tests, which monitor gas-phase indicators only while neglecting solid-phase evolution.

Table 2
Timeline of experimental stages.

Operating condition	Duration/h
Ignition and temperature-rise	1
Reverse air supply at 10 Nm³/h	7
Reverse air supply at 15 Nm³/h	9
Reverse air supply at 20 Nm³/h	7
Reverse air supply at 10 Nm³/h	10
Reverse air supply at 15 Nm³/h	9
Reverse 35% oxygen-enriched supply at 10 Nm³/h	6
Reverse 35% oxygen-enriched supply at 15 Nm³/h	6
Reverse 35% oxygen-enriched supply at 20 Nm³/h	6
Reverse air supply at 25 Nm³/h	8
Furnace shutdown	—

Upon completion of the experiment, steam was injected to cool the furnace interior. When the temperature had dropped to approximately 100°C, nitrogen was fed in to cool the system further to ambient temperature, after which the thermal-insulation plug was opened. The overlying soil layer above the simulated coal seam subsided by roughly 3 cm; this subsidence was negligible in magnitude and limited in extent.

2.4. Sampling protocol and analytical methods

Crude syngas was drawn isokinetically from the outlet manifold at each stage after the temperature record had settled to a repeatable plateau. A metered dry-gas meter recorded throughput; a water-cooled condenser collected condensate, the mass of which was recorded gravimetrically. Condensed-water samples were sealed and analysed within 24 h: pH on-site with a calibrated probe, COD by the potassium dichromate closed-reflux method, NH_3-N by Nessler reagent, oil and volatile phenols (VPs) by solvent extraction/UV, and Cl^-, SO_4^{2-} and NO_3^- by ion chromatography. Crude-gas H_2S was trapped in a cadmium-acetate impinger train and titrated; tar was collected on cooled glass-fibre thimbles and weighed. Gas composition (H_2, CH_4, CO, CO_2, O_2, N_2) was measured by thermal-conductivity and flame-ionisation GC on a daily-calibrated instrument; the NCV of each stage was computed from the dry molar composition and the lower heating value of the pure components, and is reported as MJ/Nm³ at standard conditions. Detection-limit entries are denoted by "–" in the tables. Sampling volume, condensate mass and gas throughput are stated in the table notes so that concentrations remain recognisably concentration data rather than emission inventories.

Companion-paper note. The same campaign produced the 96-thermocouple temperature field, flame-front rates and inferred cavity-growth rates; those observations are the subject of the companion paper and are not reproduced here.

2.5. Operational constraints and uncertainty statement

The ten conditions (Table 2) were run sequentially in the same 5m reactor with no intermediate purge, cool-down, or re-ignition. This maintained continuity of the developing gasification channel, combustion front, and fracture network and better reflects actual field UCG operation. Intermittent cooling or purging between stages would have caused cavity collapse, pore closure, and tar blockage, which would interrupt the reverse-combustion pathway. As a result, each stage began with a partially gasified coal seam, meaning residual carbon, porosity, and cavity geometry varied from stage to stage and differed from the initial seam condition. Every operating condition was tested a single time. No replicate datasets were collected, so standard deviations, confidence intervals, and significance tests are not available. All plotted values are point estimates from a single continuous run. The cross-stage comparisons presented below capture trends within this one test rather than results from parallel controlled experiments, and the stages should not be treated as statistically independent. These trends are specific to the time-evolving conditions of this campaign. Finally, although condensate mass and gas flowrate were recorded, recovery correction was not applied to all measured species. Only concentration-based trends are therefore reported, and no claim is made that oxygen enrichment reduces total pollutant emission.

3. Results

3.1 Syngas composition, calorific value and gasification indicators

3.1.1 Syngas composition and calorific value

Syngas composition and net calorific value (NCV) were determined for each operating condition; the results are compiled in Table 3. Under air-blown reverse gasification, the effective (H_2+CO) fraction remained within 15.53–20.34%, and the NCV did not exceed 2.76 MJ/Nm³. The high N_2 content (60.09–64.49%) diluted the combustible components and thereby limited the energy density, whereas the low oxygen partial pressure constrained the reduction reactions. The air-flow response was non-monotonic: the highest NCV (2.76 MJ/Nm³) was achieved at 15 Nm³/h, whereas at 20 Nm³/h it fell to 2.27 MJ/Nm³ despite an increased CO fraction, and at 25 Nm³/h it recovered to 2.65 MJ/Nm³ with CO rising to 7.81%. This non-monotonic behaviour indicates that, beyond a flow threshold, the benefits of an increased oxygen supply are partially offset by shortened residence time and intensified heat loss.

Under 35% oxygen enrichment, both the flow rate and product-gas quality improved. As the flow rate increased from 10 to 20 Nm³/h, H_2 concentration first rose from 15.51% to 23.39% and then levelled off at 22.39%, whereas CO increased almost monotonically from 4.00% to 22.10%; NCV increased from 3.14 to 5.98 MJ/Nm³ and the effective (H_2+CO) fraction rose from 19.51% to 44.49%. The pronounced CO surge at 20 Nm³/h indicates the onset of dominant water-gas and Boudouard reduction reactions, promoted by contraction of the oxidation zone and an elevated reduction-zone temperature. CH_4 remained consistently higher under oxygen enrichment (2.18–2.70%) than under air (1.22–1.48%), reflecting the competition between volatile-matter pyrolysis and reforming at elevated temperatures. In addition, the residual O_2 in the product gas (0.90–1.53%) suggests that the oxidant was not fully consumed, leaving room for further optimisation of oxygen supply.

Table 3
Syngas components and net calorific value under various gasification conditions (average values).

Operating condition	H_2 (%)	CH_4 (%)	CO (%)	CO_2 (%)	O_2 (%)	N_2 (%)	NCV MJ/Nm^3
Air, 10Nm^3/h	13.07	1.48	4.99	17.77	1.12	61.56	2.57
Air, 15 Nm^3/h	13.85	1.27	6.49	16.98	1.31	60.09	2.76
Air, 20 Nm^3/h	10.17	1.39	5.36	17.40	1.18	64.49	2.27
Air, 25 Nm^3/h	11.47	1.22	7.81	16.08	1.47	61.96	2.65
35% oxygen-enrichment, 10 Nm^3/h	15.51	2.70	4.00	27.39	1.53	48.86	3.14
35% oxygen-enrichment, 15 Nm^3/h	23.39	2.36	11.58	22.29	0.90	38.75	4.82
35% oxygen-enrichment, 20 Nm^3/h	22.39	2.18	22.10	16.13	0.92	36.28	5.98

3.1.2 Comparison of gasification indicators during the experiment

A series of gasification indicators were derived from the physical-model experiments including gasification-agent consumption per kilogram of coal, coal and gas consumption per 1000 Nm^3 of syngas, gas yield per kilogram of coal and calorific-value consumption of the syngas. These indicators, together with the basic coal-property parameters, were used to calculate the gasification performance under each condition; the full set of performance parameters for the reverse-air-supply tests is compiled in Table 4.

Table 4
Gasification indicators under reverse air supply conditions.

GA	Volume flow	Consumption per 1000 Nm^3 syngas			SPY	Syngas yield per kg coal		Coal consumption per 1000 kcal NCV		
		Coal /kg	Air /Nm^3	Oxygen /Nm^3	Nm^3/ kg	Air /Nm^3	Oxygen /Nm^3	Air /Nm^3	Oxygen /Nm^3	Coal /kg
Air	10Nm^3/h	291.34	787.40	/	3.43	2.70	1.28	/	0.47	1.28
	15Nm^3/h	320.41	775.19	/	3.12	2.42	1.17	/	0.48	1.17
	20Nm^3/h	279.17	833.33	/	3.58	2.99	1.54	/	0.51	1.54
	25Nm^3/h	297.12	798.72	/	3.37	2.69	1.26	/	0.47	1.26
Oxygen-enriched	10Nm^3/h	395.52	611.94	134.33	2.53	1.55	0.81	0.18	0.53	0.81
	15Nm^3/h	435.15	514.64	112.97	2.30	1.18	0.45	0.10	0.38	0.45
	20Nm^3/h	476.06	461.97	101.41	2.10	0.97	0.32	0.07	0.33	0.32

3.2 Pollutant distribution

3.2.1 Pollutants in condensed water

The high-temperature crude syngas discharged from the gasifier was cooled in a heat exchanger, so that the water vapour contained in the syngas condensed into liquid water. After separation by a gas-water separator, the condensed water was collected and subjected to conventional analyses to determine the pollutant concentrations. The results are summarised in Table 5.

Table 5
Pollutant concentrations in condensed water of crude syngas.

Operating condition	PH	COD	NH_3-N	Oil	VPs	Cl^-	SO_4^{2-}	NO_3^-
		mg/L	mg/L	mg/L	mg/L	mg/L	mg/L	mg/L
Air, 10Nm^3/h	4.28	4063	2148.67	1595.00	582.17	190.6	2400	110
Air, 15Nm^3/h	8.18	4349	3245.96	1140.85	1219.78	3	30	-
Air, 20Nm^3/h	8.23	6035	3363.89	1565.43	1497.00	22	120	-
Air, 25Nm^3/h	8.84	99330	4468.63	4813.80	3465.28	3.2	20	-
35% oxygen enrichment, 10 Nm^3/h	7.86	4996	3245.96	635.77	1247.50	3.3	30	-
35% oxygen enrichment, 20 Nm^3/h	8.69	12040	3041.15	4862.29	2744.50	9.8	80	-

"-" denotes value below the detection limit. ¹ The COD value under air condition of 25 Nm³/h is a late-stage non-steady result, not representative of steady-state gasification performance.

According to the Class III discharge limits for second-class pollutants specified in the Integrated Wastewater Discharge Standard (GB 8978 – 1996), the maximum permissible discharge concentrations are: pH 6–9, chemical oxygen demand (COD) 1000 mg/L, volatile phenols 2.0 mg/L. The concentrations of these pollutants in the coal-gas condensate all substantially exceed the national limits, indicating that effective treatment is indispensable before discharge.

3.2.2 Pollutants in crude syngas

The high-temperature crude syngas produced by the gasifier was cooled in a gas-washing bottle, after which the concentrations of hydrogen sulfide (H_2S) and tar were measured. The corresponding results are presented in Table 6.

Table 6
Pollutant contents in crude coal gas.

Process Conditions	H_2S (mg/m^3)	Tar (g/m^3)
Air 10Nm^3/h	-	6.07
Air 15Nm^3/h	554.33	-
Air 20Nm^3/h	624.70	5.61
Air 25Nm^3/h	602.00	2.89
35% oxygen-enrichment 10Nm^3/h	795.57	-
35% oxygen-enrichment 15Nm^3/h	1464.14	6.49
35% oxygen-enrichment 20Nm^3/h	1070.87	7.80

Most UCG studies characterize wastewater pollutants (phenols, COD, NH_3-N, heavy metals) and crude-gas pollutants (H_2S, tar) in separate streams, with limited attempts to attribute pollution peaks jointly to coal properties and the in-furnace temperature field (Imran et al., 2014; Kapusta et al., 2013; Pankiewicz-Sperka et al., 2021; Stańczyk et al., 2011; Cui et al., 2014). In the present work, a coupled analytical framework incorporating coal properties, the temperature field and multiphase pollutants was established

Condensed water and crude coal gas. Under low-air-flow conditions, accumulated organic acids acidify the condensed water. By contrast, oxygen-enriched gasification generates abundant NH_3 that neutralises acidity, elevating the pH to 7.8–8.9. Volatile phenols show a strong correlation with COD and serve as the core carrier of organic pollution. At 35% oxygen enrichment, high-temperature tar cracking substantially reduces the oil load in the liquid phase compared with the high-air-flow scenario. For crude coal gas, over 90% of sulfur in lignite is converted into H_2S. The 35% oxygen-enriched condition at 15 Nm³/h forms the longest high-temperature zone, facilitating thorough sulfur release and achieving the highest H_2S concentration across all tests. An increase in flow rate dilutes H_2S by the oxidant, while the tar content keeps rising.

The results indicate that low-oxygen enrichment improves gas-production quality without reducing the total release of pollutants. Targeted purification schemes are therefore proposed, including in-situ desulphurisation, catalytic tar cracking and advanced treatment of phenolic wastewater, together with a comprehensive engineering environmental-risk assessment system to address the gap in supporting environmental solutions in existing research.

4. Discussion

Two caveats constrain the pollution analysis. First, only pollutant concentrations referenced to their respective sampling bases are obtained. Without a species inventory corrected by mass recovery, the claim that “oxygen enrichment reduces total pollutant release” cannot be justified and is therefore omitted throughout this work. Second, the 35% O_2, 15 Nm³/h test yields the maximum H_2S concentration (1464 mg/m³) observed in the entire experimental campaign. Accordingly, labelling this condition as “environmentally preferable” would conflict with the environmental evaluation criterion; this designation is not adopted. Field-scale validation of UCG has been

demonstrated in operating mines; a 60-day pilot trial at the Wieczorek coal mine (Poland) confirmed that the process can be conducted safely using a V-shaped gasification channel, with controllable primary parameters and a detailed mass balance (Mocek et al., 2016).

4.1 The low-oxygen-enrichment window: position and economics

Most published UCG studies related to oxygen gradients focus on pure air or oxygen content above 40%. Systematic experimental data for the 21–35% oxygen range remain scarce, and our work fills this research gap.

At 35% oxygen enrichment and 20 Nm3/h, the net calorific value reached 5.98 MJ/Nm^3. This is approximately half of the 10.48–12.48 MJ/Nm^3 range reported by Su et al. for 40–70% oxygen enrichment, rather than an approach to it: the low-oxygen window (21–35%) raises NCV from the air-blown 2.27–2.76 MJ/Nm^3 band but remains far below the high-purity-oxygen regime. No field energy-yield projection is implied (Su et al., 2022).

Within this low-oxygen enrichment window (≤ 35 vol.% O_2), as the flow rate increased from 10 to 20 Nm^3/h, pure-oxygen consumption per 1000 Nm^3 of syngas dropped from 134.33 to 101.41 Nm^3 (a ~ 24.5% reduction), indicating improved oxygen utilisation at higher flow rates. These results demonstrate that low-oxygen enrichment achieves a balance among syngas quality, oxygen economy, and pollutant burden, rather than delivering a monotonic improvement (Bazaluk et al., 2021).

4.2 Pollutant-formation pathways and environmental constraints

Four major pollutant generation pathways can be summarised from measurement data:

(1) Under low-flow air-blown conditions, the condensate exhibited a low pH (4.28 at 10 Nm^3/h), consistent with acidic UCG process water reported in large-scale ex-situ tests (pH down to 4.6; Kapusta & Stańczyk, 2020). Phenolic compounds and water-soluble organics released during low-temperature pyrolysis are likely contributors (Xin et al., 2026; Smoliński et al., 2013), though the exact acidifying species require further speciation in this study.

(2) Higher flow rates and elevated oxygen concentrations increase the peak temperature and promote vapor-phase tar cracking. For instance, the tar concentration in condensate under 35 vol.% O_2 at 10 Nm^3/h (635.77 mg/L) was far lower than that under high-flow air-blown conditions (4813.80 mg/L at 25 Nm^3/h), representing an ~ 87% reduction. Nevertheless, tar carried by the crude syngas still rises with increasing flow rate (Wiatowski and Kapusta, 2020).

(3) Under oxygen-enriched conditions, ammonia derived from coal-bound nitrogen partitions into the condensate. The presence of ammonia in UCG condensate has been reported in field-scale characterisation studies (Humenick & Mattox, 1982), and coal-N conversion to NH_3 is enhanced under oxidising/gasifying conditions (Chang et al., 2004). In the present tests, this buffered the initially acidic condensate, raising the measured pH to 7.8–8.9.

(4) Complete sulfur conversion requires sufficient high-temperature reaction zones (Hu et al., 2021). The highest H_2S concentration (1464.14 mg/m³) was observed at 35 vol.% O_2 and 15 Nm³/h. At higher flow rates, oxidant dilution per unit coal and shorter gas residence time reduced the H_2S concentration, whereas tar concentration in the condensate continued to increase. Laboratory ex-situ UCG tests provide methodological context for syngas characterization under varying gasification agents (Laciak et al., 2016).

The extremely high COD value (99,330 mg/L) recorded at 25 Nm³/h under air blow is likely due to late-stage cavity expansion and incomplete tar cracking. This observation aligns with tar evolution patterns reported in pilot UCG trials (Wiatowski et al., 2020). Such high values indicate process risks rather than typical steady-state behavior. All measured pollutant concentrations surpass the Grade-III discharge limits set by GB 8978 – 1996. Moderate oxygen enrichment enhances syngas quality and process controllability, as demonstrated in field and semi-industrial trials (Wang et al., 2009; Moček et al., 2016), but our results show that it does not reduce total pollutant output. Consequently, pollutant removal units must be designed for high-flow oxygen-enriched scenarios, combining in-situ desulfurization, catalytic tar cracking, and advanced phenolic wastewater treatment (Burchart-Korol et al., 2016). Water-related environmental hazards call for a comprehensive risk assessment framework (Imran et al., 2014). Beyond end-of-pipe control, oxygen-enriched UCG syngas may also be directed toward high-value utilization routes such as SOFC-based hydrogen and power generation (Prabu & Jayanti, 2012).

4.3 Tripartite evaluation: efficiency, oxygen cost and environmental risk

Model-scale UCG tests show that raising the oxygen volume fraction from 40% to 80% increases the overall exergy efficiency from 67.47% to 78.52%, although the external exergy efficiency peaks at 60% O_2 and then declines (Shan et al., 2021). This non-linear behaviour indicates that higher oxygen enrichment does not guarantee monotonic improvement in usable energy output. To quantify the trade-offs under moderate oxygen enrichment, performance is evaluated on a common energy basis using two indicators.

The energy-recovery efficiency η_E is defined as syngas net calorific value (NCV, MJ/Nm³) multiplied by specific product yield (Nm³/kg coal) divided by coal enthalpy (GCV, MJ/kg):

$$\eta_E = \left(NCV_{sys} \times Y_{sp}\right) / H_{coal}$$

1

where NCV_{sys} is the syngas net calorific value, Y_{sp} is the specific product yield, and H_{coal} is the coal enthalpy (gross calorific value).

The oxygen-cost indicator C_{O_2} is defined as pure-oxygen consumption per unit syngas net energy

$$C_{O_2} = (V_{O_2}/1000) \cdot (1000/HV) \cdot c_{O_2} \cdot 10^{-3}$$

2

where V_{O_2} is the oxygen volume per 1000 Nm³ syngas (Nm³), HV is the syngas calorific value (MJ/Nm³; here NCV is used), c_{O_2} is the unit conversion factor (kg O_2/Nm³ at standard conditions), and 10^{-3} converts the final unit. C_{O_2} thus has units of kg O_2/GJ. This formulation follows standard energy-recovery and stoichiometric

coal-consumption evaluations in UCG, in which raising oxygen supply generally increases NCV and reduces specific oxygen demand per unit energy, while the marginal gain depends on flow rate, steam/oxygen ratio and cavity temperature.

As listed in Table 4, at 35% O_2, specific oxygen consumption decreases from 42.8 kg O_2/GJ at 10 Nm³/h to 23.4 kg O_2/GJ at 15 Nm³/h and 17.0 kg O_2/GJ at 20 Nm³/h. However, environmental indicators reverse this monotonic oxygen-saving trend: H_2S peaks at 15 Nm³/h (1464.14 mg/m³) and remains elevated at 1070.87 mg/m³ at 20 Nm³/h; crude-gas tar increases from 6.49 to 7.80 g/m³ with flow rate; more importantly, condensed-water oil jumps to 4862.29 mg/L at 20 Nm³/h (Table 5). Tar/oil condensation behaviour shows that aliphatic hydrocarbons and phenolic/aromatic organics migrate with producer gas and enrich in washing/condensate water, so high crude-gas tar and high condensed-oil loading represent a liquid-phase pollution penalty independent of gaseous NCV.

Considering these coupled energy–environment trade-offs, the 35% O_2 / 15 Nm³/h case is identified as the near-optimal compromise: NCV reaches 4.82 MJ/Nm³ (≈ 81% of the 20 Nm³/h value), with moderate H_2S, lower crude tar (6.49 vs. 7.80 g/m³), and a lower expected condensed-oil penalty than the 20 Nm³/h case. The 20 Nm³/h case delivers the highest NCV (5.98 MJ/Nm³) and lowest C_{O_2} (17.0 kg O_2/GJ) but imposes severe condensed-water organic pollution, so it is recommended only with enhanced syngas cleaning and wastewater treatment. For conventional field scenarios with balanced economy and environmental constraints, 15 Nm³/h is preferred; for high-energy-output demand, 20 Nm³/h may be adopted provided matched tar/oil/COD removal capacity is available.

The directional trends established here are bounded by the simulator geometry and scale. They motivate further investigation into pressure effects, cavity cross-section evolution, and controlled cavity-reset procedures before any field-relevant extrapolation can be claimed; no field-scale projection is asserted in this study.

5. Conclusions

1. Effect of Oxygen Enrichment on Gasification Efficiency and Oxygen Consumption

Oxygen enrichment significantly increased the syngas NCV from a baseline of 2.27–2.76 MJ/Nm³ to 5.98 MJ/Nm³; however, this value remains at approximately 50% of the typical range reported for established UCG operations (10.48–12.48 MJ/Nm³). Meanwhile, specific oxygen consumption can be reduced to approximately 42.8 Nm³/GJ under optimised operating conditions, indicating a quantifiable trade-off between improved gas quality and reduced oxygen demand.

2. Quality–Environment Trade-off and Pollutant Release Patterns

The improvement in syngas quality carries clear environmental trade-offs: H_2S concentration (peaking at 1464 mg/m³), condensate COD, and tar content all increased with higher oxygen enrichment levels and flow rates. Available data only support a positive correlation at the concentration level and cannot confirm that oxygen enrichment reduces total pollutant release; therefore, the oxygen enrichment process does not possess an intrinsic pollutant mitigation effect.

3. Carbon Closure and Weight Sensitivity in Multi-Objective Decision-Making

Carbon closure based on CO + CO_2 + CH_4 was 86–90%; residual carbon was retained as an uncertainty rather than corrected, reflecting an inherent limitation in carbon conversion during gasification. Min–max normalised screening across efficiency, oxygen cost, and environmental risk demonstrated that the optimal operating condition is strongly dependent on weight allocation: equal weights favoured 35% O_2, 15 Nm^3/h, while doubling the environmental weight shifted the preference to 35% O_2, 10 Nm^3/h. This outcome is essentially a weight-dependent conditional compromise rather than an absolute optimum.

Declarations

Conflict of Interest

The authors declare that they have no known competing financial interests or personal relationships that could have appeared to influence the research work reported in this paper. No funding or sponsorship was received that would affect the outcome or interpretation of the results. All authors have read and approved the manuscript for publication.

Ethics Declaration

This study does not involve human participants, human data, or animal experiments. The research design and experimental procedures in this study comply with the ethical standards and academic guidelines of the journal and the relevant national scientific research regulations. No ethical conflicts or potential moral risks exist in this work.

Funding

This work was supported by the Guizhou Provincial Scientific and Technological Program “Guizhou Key Laboratory of Coal Fluidized Mining” (Grant No. ZDSYS[2023]002), the Guizhou Provincial Key Technology R&D Program (Grant No. [2025] General 067), and the Scientific Research Project of Guizhou Provincial Coalfield Geology Bureau (Grant No. [2024] 1–03).

Author Contribution

Y. Li designed the experiments, performed the investigations, and wrote the original draft. Z. Jiang developed the numerical model, conducted the simulations, and validated the results. L. Qian assisted with the experiments and data analysis. L. Wang supervised the project, acquired funding, and reviewed and edited the manuscript. All authors read and approved the final version.

Acknowledgement

This research was supported by the Guizhou Provincial Scientific and Technological Program “Guizhou Key Laboratory of Coal Fluidized Mining” (No. ZDSYS[2023]002), the Guizhou Provincial Key Technology R&D Program (No. [2025] General 067)., the Scientific Research Project of Guizhou Provincial Coalfield Geology Bureau (No. [2024] 1-03).

Data Availability

All data generated or analyzed during this study are fully available and included in this published article. The raw and processed data supporting the findings of this study are available from the corresponding author upon reasonable request. There are no restrictions on data availability.

References

1. Bazaluk, O. et al. Experimental studies of the effect of design and technological solutions on the intensification of an underground coal gasification process. *Energies* **14**, 4369. 10.3390/en14144369 (2021).
2. Burchart-Korol, D., Krawczyk, P., Czaplicka-Kolarz, K. & Smoliński, A. Eco-efficiency of underground coal gasification (UCG) for electricity production. *Fuel* **173**, 239–246. 10.1016/j.fuel.2016.01.019 (2016).
3. Chang, L. P., Xie, K. C. & Li, C. Z. Release of fuel-nitrogen during the gasification of Shenmu coal in O_2. Fuel Process. Technol. 85(8–10), 1053–1063; (2004). 10.1016/j.fuproc.2003.11.038
4. Cui, Y. et al. Forward and reverse combustion gasification of coal with production of high-quality syngas in a simulated pilot system for in situ gasification. *Appl. Energy*. **131**, 9–19. 10.1016/j.apenergy.2014.06.001 (2014).
5. DAN, P. et al. Exergy analysis of underground coal gasification with different oxygen concentrations. *J. China Coal Soc.* **46** (8), 2673–2680. 10.13225/j.cnki.jccs.2020.0631 (2021).
6. Ding, J. et al. Research on the underground gasification of lignite through an oxygen enrichment process: insights from experimental study and Aspen Plus process model. *RSC Adv.* **14**, 36398–36409. 10.1039/d4ra06654e (2024).
7. Dong, M. et al. Inhibitory effect of novel swirl flow injection technology on tar pollutant formation in underground coal gasification: experiments and numerical simulation. *J. Environ. Chem. Eng.* **14**, 120714. 10.1016/j.jece.2025.120714 (2026a).
8. Dong, M. et al. Kinetic and thermodynamic evolution driven by oxygen gradients in underground coal gasification. *Fuel* **427**, 139693. 10.1016/j.fuel.2026.139693 (2026b).
9. Huang, W., Wang, Z., Duan, T. & Xin, L. Effect of oxygen and steam on gasification and power generation in industrial tests of underground coal gasification. *Fuel* **289**, 119855. 10.1016/j.fuel.2020.119855 (2021).
10. Hu, Z., Peng, Y., Sun, F., Chen, S. & Zhou, Y. Thermodynamic equilibrium simulation on the synthesis gas composition in the context of underground coal gasification. *Fuel* **293**, 120462. 10.1016/j.fuel.2021.120462 (2021).
11. Humenick, M. J. & Mattox, C. F. Characterization of condensates produced during underground coal gasification. In Situ 6(1), 1–27. (1982).

12. Imran, M. et al. Environmental concerns of underground coal gasification. *Renew. Sustain. Energy Rev.* **31**, 600–610 (2014).
13. Laciak, M., Kostúr, K., Durdán, M., Kačur, J. & Flegner, P. The analysis of the underground coal gasification in experimental equipment. *Energy* **114**, 332–343. 10.1016/j.energy.2016.08.004 (2016).
14. Pankiewicz-Sperka, M., Kapusta, K., Basa, W. & Stolecka, K. Characteristics of water contaminants from underground coal gasification (UCG) process—effect of coal properties and gasification pressure. *Energies* **14**, 6533. 10.3390/en14206533 (2021).
15. Perkins, G. & Vairakannu, P. Considerations for oxidant and gasifying medium selection in underground coal gasification. Fuel Process. Technol. 165, 145–154; (2017). 10.1016/j.fuproc.2017.05.010
16. Sadasivam, S. et al. Characterisation of the Contaminants Generated from a Large-Scale Ex-Situ Underground Coal Gasification Study Using High-Rank Coal from the South Wales Coalfield. *Water Air Soil. Pollut*. **231**, 519. 10.1007/s11270-020-04888-1 (2020).
17. Smoliński, A., Stańczyk, K., Kapusta, K. & Howaniec, N. Analysis of the organic contaminants in the condensate produced in the in situ underground coal gasification process. *Water Sci. Technol.* **67** (3), 644–650. 10.2166/wst.2012.558 (2013).
18. Stańczyk, K. et al. Gasification of lignite and hard coal with air and oxygen enriched air in a pilot scale ex situ reactor for underground gasification. *Fuel* **90** (5), 1953–1962. 10.1016/j.fuel.2010.12.007 (2011).
19. Su, F. et al. Impact of O_2-enriched CO_2 blending ratios on energy efficiency and carbon abatement in underground coal gasification. Energy 339, 139064; (2025). 10.1016/j.energy.2025.139064
20. Su, F. et al. Energy recovery evaluation and temperature field research of underground coal gasification under different oxygen concentrations. *Fuel* **329**, 125389. 10.1016/j.fuel.2022.125389 (2022).
21. Wang, Z., Huang, W., Zhang, P. & Xin, L. A contrast study on different gasifying agents of underground coal gasification at Huating Coal Mine. *J. Coal Sci. Eng. (China)*. **17**, 181–186. 10.1007/s12404-011-0214-1 (2011).
22. Wiatowski, M. & Kapusta, K. Evolution of tar compounds in raw gas from a pilot-scale underground coal gasification (UCG) trial at Wieczorek mine in Poland. *Fuel* **276**, 118070. 10.1016/j.fuel.2020.118070 (2020).
23. Xin, L. et al. Precipitation pattern of typical organic pollutants in wastewater during underground coal gasification process. *J. China Coal Soc.* **51** (2), 1698–1706. 10.13225/j.cnki.jccs.QH25.0117 (2026).

Figures



Figure 1

On-site photograph showing the cross-section of the coal-seam layout.

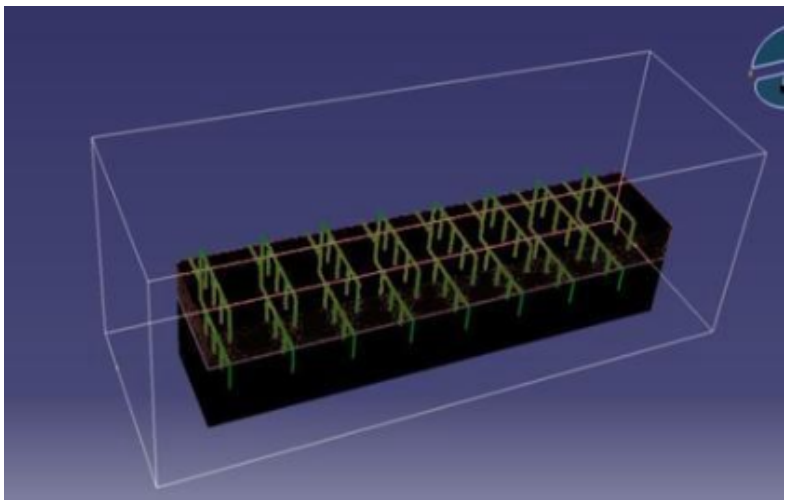

Figure 2

Schematic diagram of thermocouple arrangement inside the furnace.